Evaluation of the Stretched-Vortex Subgrid-Scale Model for Large-Eddy Simulation with a Fourth-Order Finite Volume Algorithm

Sean Walters*, Xinfeng Gao†, and Stephen Guzik‡
Computational Fluid Dynamics and Propulsion Laboratory
Colorado State University, Fort Collins, CO 80523, USA

The stretched-vortex subgrid-scale model for large-eddy simulation is implemented in a fourth-order finite volume algorithm designed for compressible flows. Various forms of the model are tested using the Taylor-Green vortex case and the results are compared with one another for the purpose of evaluating the models in a non-spectral finite volume context.

Nomenclature

ρ	mass density
$\vec{u}$	velocity vector
e	total specific energy
p	pressure
T	temperature
$\vec{q}$	molecular heat flux vector
$\vec{\vec{\tau}}$	molecular stress tensor
μ	dynamic viscosity
ν	kinematic viscosity
ϵ	energy dissipation rate
κ	spectral wavenumber
κ_c	wavenumber cutoff
Δ_c	physical cutoff length
$\mathcal{K}_0$	Kolmogorov prefactor
λ	eigenvalue
σ	weighting factor
F_2	second-order structure function
$\Gamma(\cdot)$	incomplete gamma function
ϕ	scalar quantity
$\vec{\phi}$	spatial vector
$\boldsymbol{\phi}$	state vector
$\vec{\vec{\phi}}$	tensor
$\bar{\phi}$	filtered quantity
$\tilde{\phi}$	Favre-filtered quantity
$\vec{x}$	physical space, e.g., (x, y, z)
$\Delta x, \Delta y$	spatial step

I. Introduction

In the large-eddy simulation (LES) paradigm of computational fluid dynamics (CFD), the simulation resolves large eddies while modeling small-scales. Clearly, a separation of physical scales forms the mathematical foundation upon which LES is built and understood. While the specifics of this foundation depend on the type of filter chosen, the resulting analytical form of the filtered equations has a certain level of universality independent of the chosen filter. At the most general level of consideration, the filtering process separates a data field, ϕ, into two portions. For the purpose of LES, the scale-separator is typically chosen as a low-pass filter which separates the low-frequency field component, $\bar{\phi}$, which is discretely resolved, from the high-frequency component, ϕ', the effect of which is modeled. This process invokes a decomposition-type definition for the field of interest

$$\phi = \bar{\phi} + \phi' \ .$$

Going beyond generalities, the definition of the filter itself would be expected to make a difference in further developments of the LES scheme. Two general classes of filtering operations are traditionally defined

*Graduate Research Assistant, Email: walters2@rams.colostate.edu, Student Member AIAA
†Associate Professor, Email: xinfeng.gao@colostate.edu, Member AIAA
‡Assistant Professor, Email: stephen.guzik@colostate.edu, Member AIAA

within LES: convolution filters and differential filters. Although much of the existing LES literature contrasts convolution and differential filters, it has been known for some time that these are two forms of the same filtering process and are linked through an inverse problem.[1,2] With this in mind, a general form of the filtered governing equations can be derived for and reasonably applied to both filter forms. This helps to separate some of the initial model development process from the class of filter chosen.

An additional level of filter distinction involves whether or not the filter is a linear or nonlinear operator. An operator, $\mathcal{L}$, is defined as linear if, when applied to variables ϕ and ψ and scalar constant α, it satisfies

$$\mathcal{L}\left(\phi+\psi\right)=\mathcal{L}\left(\phi\right)+\mathcal{L}\left(\psi\right) \quad , \quad \mathcal{L}\left(\alpha\phi\right)=\alpha\mathcal{L}\left(\phi\right) \ . \tag{1}$$

Another consideration regards whether the filter will be applied to the compressible Navier-Stokes equations and whether it will be a Favre-averaging type of filter. Favre-averaging allows the decoupling of density from the majority of the nonlinearities in such a way that the equation of mass conservation does not require a subfilter scale model. The Favre-filtering process is defined by

$$\tilde{\phi}=\frac{\overline{\rho\phi}}{\bar{\rho}} \ , \tag{2}$$

where $\bar{\rho}$ is the mass density filtered with the non-Favre type filter chosen.

Neglecting nonlinear filters and only focusing on Favre-filtering with linear filters, the compressible Navier-Stokes equations can be written as[3]

$$\frac{\partial\bar{\rho}}{\partial t}+\boldsymbol{\nabla}\cdot\left(\bar{\rho}\tilde{\vec{u}}\right)=0 \, , \tag{3}$$

$$\frac{\partial}{\partial t}\left(\bar{\rho}\tilde{\vec{u}}\right)+\boldsymbol{\nabla}\cdot\left(\bar{\rho}\tilde{\vec{u}}\tilde{\vec{u}}^{\top}+\bar{p}\vec{\vec{I}}\right)=\boldsymbol{\nabla}\cdot\tilde{\vec{\vec{\tau}}}+\mathcal{A}_1+\mathcal{A}_2 \, , \tag{4}$$

$$\frac{\partial}{\partial t}\left(\bar{\rho}\tilde{e}\right)+\boldsymbol{\nabla}\cdot\left[\bar{\rho}\tilde{\vec{u}}\left(\tilde{e}+\frac{\bar{p}}{\bar{\rho}}\right)\right]=\boldsymbol{\nabla}\cdot\left(\tilde{\vec{\vec{\tau}}}\cdot\tilde{\vec{u}}\right)-\boldsymbol{\nabla}\cdot\tilde{\vec{q}}+\mathcal{E}_1+\mathcal{E}_2+\mathcal{E}_3+\mathcal{E}_4 \, , \tag{5}$$

where $\vec{\vec{I}}$ is the identity matrix, and $\tilde{\vec{\vec{\tau}}}$ and $\tilde{\vec{q}}$ are the resolved molecular stress tensor and the resolved molecular heat flux vector. In addition, $\tilde{\vec{u}}^{\top}$ is the transpose of the filtered velocity vector. The resolved molecular fluid stress tensor is defined as

$$\tilde{\vec{\vec{\tau}}}=2\mu\left(\tilde{\vec{\vec{S}}}-\frac{1}{3}\left(\boldsymbol{\nabla}\cdot\tilde{\vec{u}}\right)\vec{\vec{I}}\right) \ , \ \tilde{\vec{\vec{S}}}=\frac{1}{2}\left(\boldsymbol{\nabla}\tilde{\vec{u}}+\left(\boldsymbol{\nabla}\tilde{\vec{u}}\right)^{\top}\right) \ . \tag{6}$$

In the governing equations, terms $\mathcal{A}_i$, and $\mathcal{E}_i$ correspond to sub-analytical-filter-scale (SAS) quantities, and result from filtering the equations. In practice, these may match subgrid-scale (SGS) terms if only a grid filter is applied. These terms are given as

$$\mathcal{A}_1=-\boldsymbol{\nabla}\cdot\left[\bar{\rho}\left(\widetilde{\vec{u}\vec{u}^{\top}}-\tilde{\vec{u}}\tilde{\vec{u}}^{\top}\right)\right] \, , \tag{7}$$

$$\mathcal{A}_2=-\boldsymbol{\nabla}\cdot\left(\overline{\vec{\vec{\tau}}}-\tilde{\vec{\vec{\tau}}}\right) \, , \tag{8}$$

$$\mathcal{E}_1=-\boldsymbol{\nabla}\cdot\left(\overline{\rho\vec{u}e}-\bar{\rho}\tilde{\vec{u}}\tilde{e}\right) \, , \tag{9}$$

$$\mathcal{E}_2=-\boldsymbol{\nabla}\cdot\left(\overline{\vec{u}p}-\tilde{\vec{u}}\bar{p}\right) \, , \tag{10}$$

$$\mathcal{E}_3=\boldsymbol{\nabla}\cdot\left(\overline{\vec{\vec{\tau}}\cdot\vec{u}}-\tilde{\vec{\vec{\tau}}}\cdot\tilde{\vec{u}}\right) \, , \tag{11}$$

$$\mathcal{E}_4=-\boldsymbol{\nabla}\cdot\left(\bar{\vec{q}}-\tilde{\vec{q}}\right) \, , \tag{12}$$

and are correction factors that arise after applying a scale separator to the nonlinear terms in the governing equations. To close the LES system, these terms must be modeled. Of these terms, $\mathcal{A}_1$ has received the most in-depth treatment due to its appearance as the sole nonlinearity in typical incompressible LES formulations. An incompressible LES scheme which tracks temperature through a decoupled energy equation could also deal with the $\mathcal{E}_1$ and $\mathcal{E}_2$ terms re-written as functions of temperature. This detail is of some potential importance to compressible LES formulations.

The correction terms presented can be approximated using functional models, structural models, or a deconvolution-convolution type model. Within this paper, a structural model is utilized for approximating these correction terms.

II. Stretched Spiral-Vortex SGS Model

II.A. Historical background

The model under consideration in this paper, the stretched-vortex subgrid/sub-analytical-scale (SVS) model, is a *true* structural LES SGS model. That is, it is based on the assumption that, at sufficiently high Reynolds numbers and sufficiently small length scales, there exists a known flow structure guiding the evolution of kinetic energy in the flow. Quantifying this structure and developing an SGS model from it is intended to provide an LES model applicable to a flow of interest.

Following Kolmogorov's seminal 1941 paper, researchers sought a flow configuration providing the kinetic energy spectrum that Kolmogorov predicted would appear in the limit of infinite Reynolds numbers.[4] Until Lundgren's 1982 paper, no analytical Navier-Stokes solutions were identified which gave the -5/3 power energy spectrum.[5] Lundgren's approach to a solution began with the incompressible formulation of the Navier-Stokes equations and a structure commonly encountered in shear flow problems: the spiral vortex. A double-shear flow configuration with typical spiral vortices is depicted in Figure 1. Lundgren was not

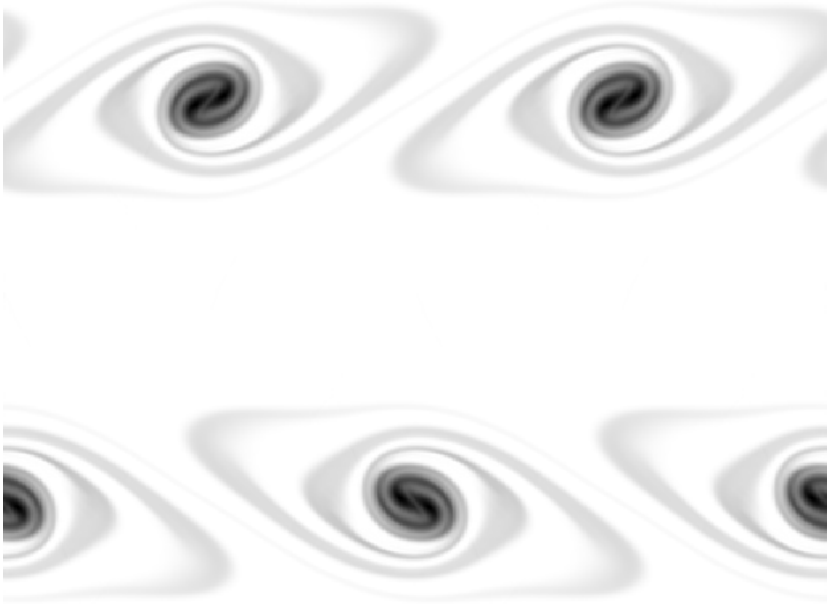

Figure 1: Spiral vortices created in double shear flow (Yijun Wang, personal communication).

the first to propose this structure for fine-scale turbulence.[6] However, after including vortex-strain in the model and time-averaging the solution over the duration of the vortex lifetime, he arrived at a spectrum with the desired -5/3 power. An exponential scaling coefficient is the only difference between Lundgren's energy spectrum and the Kolmogorov spectrum. Lundgren's spectrum is written as

$$E(\kappa) = \mathcal{K}_0 \epsilon^{2/3} \kappa^{-5/3} \exp\left(-2\kappa^2 \nu / (3|\tilde{a}|)\right) \ , \tag{13}$$

where κ is the wavenumber, $\mathcal{K}_0$ is the Kolmogorov prefactor, ϵ is the energy dissipation rate, ν is the kinematic viscosity of the fluid, and $\tilde{a}$ is the stretching of the subgrid-vortex by the resolved field.

II.B. Initial development

With an interest in universal descriptions of the fine scales of turbulence, Saffman and Pullin further investigated Lundgren's model throughout the 1980's and 1990's.[7–10] The eventual result of this work was Misra and Pullin's 1997 paper detailing a stretched-vortex subgrid-scale LES model used within a psuedo-spectral algorithm.[11] Misra and Pullin's resulting model approximated the subgrid stress-tensor through an

approximation of the subgrid kinetic energy, K, and the orientation vector, $\vec{e^v}$, of the subgrid vortices. After approximating the orientation vector using products of delta functions, the model was presented as

$$\left(\overline{\vec{u}\vec{u}^\top} - \bar{\vec{u}}\bar{\vec{u}}^\top\right) = K\left(\vec{\vec{I}} - \vec{e^v}\left(\vec{e^v}\right)^\top\right) \ , \tag{14}$$

where $\vec{\vec{I}} - \vec{e^v}\vec{e^v}$ is a generalized form of an ensemble average of the probability density function (PDF) describing the orientation of the subgrid vortices. In Misra's paper, K was assumed to have the Kolmogorov spectrum

$$E\left(\kappa\right) = \mathcal{K}_0 \epsilon^{2/3} \kappa^{-5/3} \ , \tag{15}$$

and was determined using a nonlocal procedure well suited for a psuedo-spectral code.

Additionally, three models were proposed for the ensemble averaged PDF of the orientation vector of the subgrid vortices. It is apparent from the model form that the estimation of the subgrid vortex orientation vector is as important or potentially more important than the estimation of the subgrid kinetic energy. Disallowing negative subgrid kinetic energy, the orientation vector is the only factor determining the sign of this model and whether it is dissipative or anti-dissipative in nature.

The first of the three models, model (1a), was based on the strongest and second-strongest eigenvectors of the local strain-rate tensor, denoted as $\vec{e^3}$ and $\vec{e^2}$ respectively. Taking the form

$$\left(\overline{\vec{u}\vec{u}^\top} - \bar{\vec{u}}\bar{\vec{u}}^\top\right) = K\left[\sigma\left(\vec{\vec{I}} - \vec{e^3}\left(\vec{e^3}\right)^\top\right) + (1-\sigma)\left(\vec{\vec{I}} - \vec{e^2}\left(\vec{e^2}\right)^\top\right)\right] \ , \tag{16}$$

it allowed for unequal weighting to be applied to the eigenvectors through the weighting parameter σ. It was reported that this model provided no resulting backscatter in kinetic energy from the fine turbulent scales to the largest turbulent scales, in contrast with direct numerical simulations (DNS).

The second orientation model which Misra proposed, model (1b), again included the strongest eigenvector of the local strain-rate tensor. However, instead of relying on the second-strongest eigenvector of the strain-rate tensor, it relied on the local, resolved vorticity vector, denoted $\vec{e^\omega}$. This naturally follows if one assumes that the breakdown of the resolved vortices generates the subgrid vortices. Similar to the first model, the second model was presented as

$$\left(\overline{\vec{u}\vec{u}^\top} - \bar{\vec{u}}\bar{\vec{u}}^\top\right) = K\left[\sigma\left(\vec{\vec{I}} - \vec{e^3}\left(\vec{e^3}\right)^\top\right) + (1-\sigma)\left(\vec{\vec{I}} - \vec{e^\omega}\left(\vec{e^\omega}\right)^\top\right)\right] \ , \tag{17}$$

and was reported to provide slightly more energy backscatter than the first model.

Misra's third model, model (2), was of a significantly different form than the first two models. Formulated as a time-dependent ordinary differential equation (ODE), the model tracks the evolution of the subgrid-scale vorticity vector over time. The model, given by,

$$\frac{\partial \vec{e^v}}{\partial t} = \left(\boldsymbol{\nabla}\bar{\vec{u}}\right)\vec{e^v} - \vec{e^v}\left(\vec{e^v}\right)^\top\left(\boldsymbol{\nabla}\bar{\vec{u}}\right)\vec{e^v} \ , \tag{18}$$

was reported to provide significant backscatter, exceeding the level reported in many DNS simulations. While many further papers report on the results provided by models (1a) and (1b), no further studies provide results derived from the third model, model (2). Several later papers truncated models (1a) and (1b) to a single-direction model based only on the principal eigenvector of the strain-rate tensor[12]

$$\left(\overline{\vec{u}\vec{u}^\top} - \bar{\vec{u}}\bar{\vec{u}}^\top\right) = K\left(\vec{\vec{I}} - \vec{e^3}\left(\vec{e^3}\right)^\top\right) \ . \tag{19}$$

However, it was concluded that this model tended to damp out lower, resolved, wavenumbers more than the original two-vector models.[13,14]

Misra and Pullin's 1997 paper suggested how one could potentially extend the SVS model calculation of subgrid kinetic energy to physical space. Voelkl and Pullin finished this extension to physical space algorithms through the use of a local, structure-function matching procedure that provided the subgrid kinetic energy.[15]

II.C. Subgrid scalars and compressible extensions

In addition to Lundgren's original stretched-vortex analysis, Pullin and Lundgren analyzed the effect of allowing for axial flow of velocity through the subgrid-scale vortices and allowing for associated scalar transport. Their findings matched previous theoretical work quite well and motivated further developments in the SVS model.[16] In addition to developing a model for the SGS stress-tensor, Pullin developed an SGS model for passively transported scalars using a simplified form of the analysis that he and Lundgren used in their 2001 paper.[17]

Assuming that a passive scalar is wound around the vortex, Pullin derived a model of the form

$$\overline{\phi\vec{u}} - \bar{\phi}\bar{\vec{u}} = \frac{\Delta}{2} K^{1/2} \left(\vec{\vec{I}} - e^{\vec{v}} \left(e^{\vec{v}} \right)^{\top} \right) \boldsymbol{\nabla} \bar{\phi} \ , \tag{20}$$

where Δ is the local mesh spacing. Kosovic later used these ideas to develop an extension for compressible flows.[18] Assuming that the temperature and pressure fields are passive scalars, models can be developed for terms $\mathcal{E}_1$ and $\mathcal{E}_2$ as presented in Eq. 9 and 10. This extension also provided a means for modeling SGS chemical species terms arising during turbulent chemical reaction simulations.[19]

II.D. Wall models and mapped domains

Over the last decade, further advances have been made through the extension of the SVS model to LES wall-models and mapped domains. Motivated by the subgrid scalar model work, Chung and Pullin extended the original SVS model to incorporate Pullin and Lundgren's earlier analytical analysis of axial flow of velocity through subgrid vortices. The resulting model

$$\left(\overline{\vec{u}\vec{u}^{\top}} - \bar{\vec{u}}\bar{\vec{u}}^{\top} \right) = K \left(\vec{\vec{I}} - \vec{\vec{E}} \right) - \frac{\Delta}{2} K^{\frac{1}{2}} \left[\vec{\vec{E}} \left(\boldsymbol{\nabla} \bar{\vec{u}} \right) \left(\vec{\vec{I}} - \vec{\vec{E}} \right) + \left(\vec{\vec{I}} - \vec{\vec{E}} \right) \left(\boldsymbol{\nabla} \bar{\vec{u}} \right)^{\top} \vec{\vec{E}} \right] \quad , \quad \vec{\vec{E}} = e^{\vec{v}} \left(e^{\vec{v}} \right)^{\top} \tag{21}$$

further led to the development of a wall-model.[20] Since that paper, multiple wall models have been developed from the SVS framework and applied to simulations with smooth and rough walls. The extension of these models to mapped domains has allowed for the simulation of flow over airfoils and grooved cylinders.[21–23]

III. Algorithm

Within this study, the SVS model is implemented in a fourth-order finite volume algorithm. Several models are used to compute the SGS vortex orientation vector while the SGS kinetic energy is approximated using the method presented by Chung.[20] Additionally, the compressible extension proposed by Kosovic was used in these simulations to account for the nonlinearities that arise in the energy equation for compressible flows.[18] As some of these nonlinearities arise in the decoupled energy equation in incompressible flows, it is expected that these nonlinearities must be modeled irrespective of whether the flow is in the compressible or incompressible regime. Although wall models and mapped formulations of the models are not considered in the present study, immediate followup work will focus on these features of the SVS model.

III.A. Chord

Except where noted, all of the following results were obtained using the computational fluid dynamics (CFD) solver Chord.[24–28] Chord is a fourth-order, Godunov-type finite volume algorithm formulated for structured, mapped grids. Specifically designed for high-speed, turbulent flows of reacting gases, it utilizes a spatially fourth-order solution reconstruction coupled with the PPM limiter and the standard fourth-order Runge-Kutta time-marching method. Additionally designed for multi-scale flow simulations, Chord utilizes adaptive mesh refinement (AMR) to spatially and temporally refine the simulation where necessary.

III.B. SVS Kinetic Energy Estimate

Many models for computing the SGS kinetic energy have been proposed and studied.[11–13,15,20] The various drawbacks and benefits associated with different models are not considered within this research. Instead, a single model for the SGS kinetic energy computation was chosen and consistently applied.[20] This model

$$K = \frac{1}{2} \mathcal{K}_0' \Gamma \left[-\frac{1}{3}, \kappa_c^2 \right] \ , \tag{22}$$

requires the evaluation of the incomplete gamma function, $\Gamma[\cdot]$, and the grouped Kolmogorov constant, $\mathcal{K}_0'$

$$\mathcal{K}_0' = \frac{\{F_2\}}{\{Q(\kappa_c, d)\}} \ . \tag{23}$$

In Eq. 23, $\{\cdot\}$ is an ensemble average of the variables over a spatial domain Ω

$$\{\phi\} = \frac{1}{N} \sum_{\vec{x}_i \in \Omega \ ; \ \vec{x}_i \neq \vec{x}_0} \phi(\vec{x}_0, \vec{x}_i) \ . \tag{24}$$

F_2 is the second-order structure function

$$F_2 = \left(\tilde{\vec{u}}(\vec{x}_0) - \tilde{\vec{u}}(\vec{x}_i)\right) \cdot \left(\tilde{\vec{u}}(\vec{x}_0) - \tilde{\vec{u}}(\vec{x}_i)\right) \ , \tag{25}$$

where $\vec{x}_0$ is at the point of interest and $\vec{x}_i$ is anywhere inside a spatial domain, Ω, over which the ensemble average is performed. Note that $\bar{\vec{u}}$ is now replaced with $\tilde{\vec{u}}$ to indicate the Favre-filtered quantities for compressible flows. $Q(\kappa_c, d)$ is computed using

$$Q(\kappa_c, d) = 4 \int_0^{\kappa_c} \kappa^{-5/3} \mathrm{e}^{-\kappa^2} \left(1 - J_0\left(\frac{\kappa}{\kappa_c} \pi d\right)\right) \mathrm{d}\kappa \ , \tag{26}$$

where J_0 is the zeroth-order Bessel function and where d is a measure of the planar distance from a point to the SGS vortex axis

$$d = \frac{r}{\Delta_c} \quad , \quad r = \left[(\vec{x}_0 - \vec{x}_i) \cdot (\vec{x}_0 - \vec{x}_i)\right]^{1/2} \quad , \quad \Delta_c = (\Delta x \Delta y \Delta z)^{1/3} \tag{27}$$

The κ_c variable is formulated as

$$\kappa_c = \frac{\pi}{\Delta_c} \sqrt{\frac{2\nu}{3|\tilde{a}|}} \quad , \quad \tilde{a} = \left(\vec{e^v}\right)^\top \tilde{\vec{\vec{S}}} \vec{e^v} \quad , \quad \nu = \frac{\mu}{\rho} \tag{28}$$

Efficient means of computing $\mathcal{K}_0$, evaluating $\Gamma[\cdot]$, and performing the eigenvalue/eigenvector computation are presented by Voelkl and others.[15,20,29]

III.C. SVS Vortex Orientation Models

The results in this paper are based on Misra's model (1b) as presented in Eq. 17, the simplified one-direction model as presented in Eq. 19, and an additional model as presented below.

Starting with a definition of eigenvectors of the strain-rate tensor $\tilde{\vec{\vec{S}}}$

$$\tilde{\vec{\vec{S}}} \vec{e} = \lambda \vec{e} \, , \tag{29}$$

where λ is an eigenvalue of $\vec{\vec{S}}$ and $\vec{e}$ is an eigenvector of $\vec{\vec{S}}$, it is apparent that the single-vector model presented in Eq. 19 can be re-written, using Eq. 29 and noting that the strain-rate tensor is symmetric, as

$$\vec{\vec{I}} - \frac{1}{\lambda^2} \tilde{\vec{\vec{S}}} \vec{e} \vec{e}^\top \tilde{\vec{\vec{S}}} = \vec{\vec{I}} - \vec{e}\vec{e}^\top \ . \tag{30}$$

Multiplying through by λ^2, rearranging slightly, and inserting into the full model form, a result is obtained that appears similar to the compressible molecular stress tensor given in Eq. 6

$$\left(\widetilde{\vec{u}\vec{u}^\top} - \tilde{\vec{u}}\tilde{\vec{u}}^\top\right) = -\frac{K}{\lambda^2} \left(\tilde{\vec{\vec{S}}} \vec{e} \vec{e}^\top \tilde{\vec{\vec{S}}} - \lambda^2 \vec{\vec{I}}\right) \ . \tag{31}$$

While this is certainly not surprising or even unexpected, it does give rise to some observations and questions. The identity matrix in the compressible molecular stress tensor is multiplied by the divergence of the velocity which is equivalent to the trace of the strain-rate tensor

$$\mathrm{tr}\left(\tilde{\vec{\vec{S}}}\right) = \boldsymbol{\nabla} \cdot \tilde{\vec{u}} \, . \tag{32}$$

It is also known that the trace of the strain-rate tensor is equal to the sum of the eigenvalues of the strain-rate tensor and, so, the identity matrix component in the stress tensor can be written as

$$\left(\boldsymbol{\nabla}\cdot\tilde{\vec{u}}\right)\vec{\vec{I}} = \mathrm{tr}\left(\tilde{\vec{\vec{S}}}\right)\vec{\vec{I}} = \left(\sum_i \lambda_i\right)\vec{\vec{I}}\,. \tag{33}$$

This would suggest that the λ^2 term multiplying the identity matrix in Eq. 31 acts in a closely related fashion to the divergence of velocity (the trace of the strain-rate tensor). If instead of projecting the strain-rate tensor onto its principal eigenvector, it is projected onto itself, a model somewhat akin to Clark's "gradient model" (and similar models based on the multiplication of the gradients of velocity) is obtained[30,31]

$$\left(\widetilde{\vec{u}\vec{u}^{\top}} - \tilde{\vec{u}}\tilde{\vec{u}}^{\top}\right) = -\frac{K}{c}\left(\tilde{\vec{\vec{S}}}\tilde{\vec{\vec{S}}} - c\vec{\vec{I}}\right)\,, \tag{34}$$

where c is a scaling coefficient that is expected to be related to the eigenvalues of $\tilde{\vec{\vec{S}}}\tilde{\vec{\vec{S}}}$ and is expected to normalize $\tilde{\vec{\vec{S}}}\tilde{\vec{\vec{S}}}$. The eigenvectors in $\vec{e}\vec{e}^{\top}$ are unit vectors and so it would be expected that $\tilde{\vec{\vec{S}}}\tilde{\vec{\vec{S}}}$ should function in a similar role of only providing the outer product of the normalized orientation vectors of the SGS vortices. Choosing c to be the trace of $\tilde{\vec{\vec{S}}}\tilde{\vec{\vec{S}}}$ the final form of the model becomes

$$\left(\widetilde{\vec{u}\vec{u}^{\top}} - \tilde{\vec{u}}\tilde{\vec{u}}^{\top}\right) = -K\left(\frac{1}{\mathrm{tr}\left(\tilde{\vec{\vec{S}}}\tilde{\vec{\vec{S}}}\right)}\tilde{\vec{\vec{S}}}\tilde{\vec{\vec{S}}} - \vec{\vec{I}}\right) = -K\left(\frac{1}{\|\tilde{\vec{\vec{S}}}\|^2}\tilde{\vec{\vec{S}}}\tilde{\vec{\vec{S}}} - \vec{\vec{I}}\right)\,, \tag{35}$$

where $\|\tilde{\vec{\vec{S}}}\|$ is the Frobenius norm of the strain-rate tensor.

IV. Results

The models previously discussed in this paper are tested using the Taylor-Green vortex case with initial conditions widely used for the problem and given by[32]

$$u = U_0 \sin\left(\frac{n\pi x}{D}\right)\cos\left(\frac{n\pi y}{D}\right)\cos\left(\frac{n\pi z}{D}\right) \tag{36}$$

$$v = -U_0 \cos\left(\frac{n\pi x}{D}\right)\sin\left(\frac{n\pi y}{D}\right)\cos\left(\frac{n\pi z}{D}\right) \tag{37}$$

$$w = 0 \tag{38}$$

$$p = p_0 + \frac{\rho_0 U_0^2}{16}\left(\cos\left(\frac{2n\pi x}{D}\right) + \cos\left(\frac{2n\pi y}{D}\right)\right)\left(\cos\left(\frac{2n\pi z}{D}\right) + 2\right) \tag{39}$$

$$\rho = \frac{p}{RT_0} = \frac{p\rho_0}{p_0} \tag{40}$$

where U_0 is the magnitude of the velocity fluctuation, D is the domain length in every coordinate direction (assuming a cubic domain), and n is the number of vortices contained in the domain in each coordinate direction. The flow has a Reynolds number of 1600 based on a length scale $L = D\pi/2$, a Mach number of 0.1, and a Prandtl number of 0.71. Of interest are the domain-averaged kinetic energy, enstrophy, and the kinetic energy dissipation rate. These quantities provide insight into the ability of the turbulence model to provide necessary information from features smaller than the grid cutoff size. Throughout the rest of the paper, the results are presented with respect to a non-dimensionalized time $\tau = tU_0/L$.

As a baseline for comparison, Figs. 2, 3, and 4 display the kinetic energy, enstrophy, and kinetic energy dissipation rate when turbulence models are not utilized. Two of the cases presented are derived from datasets that have been averaged down from resolutions of 256^3 and 128^3 to 64^3. In each of these cases, fine grid simulations were computed and the resulting conservative-variable solution fields were averaged to 64^3 resolution. The other two cases presented were run at a resolution of 64^3 with and without the PPM limiter.

The second set of figures, Figs. 5, 6, and 7 show the results with the turbulence models and with the PPM limiter, while the third set, Figs. 8, 9, and 10 show the results with the turbulence models and without the PPM limiter.

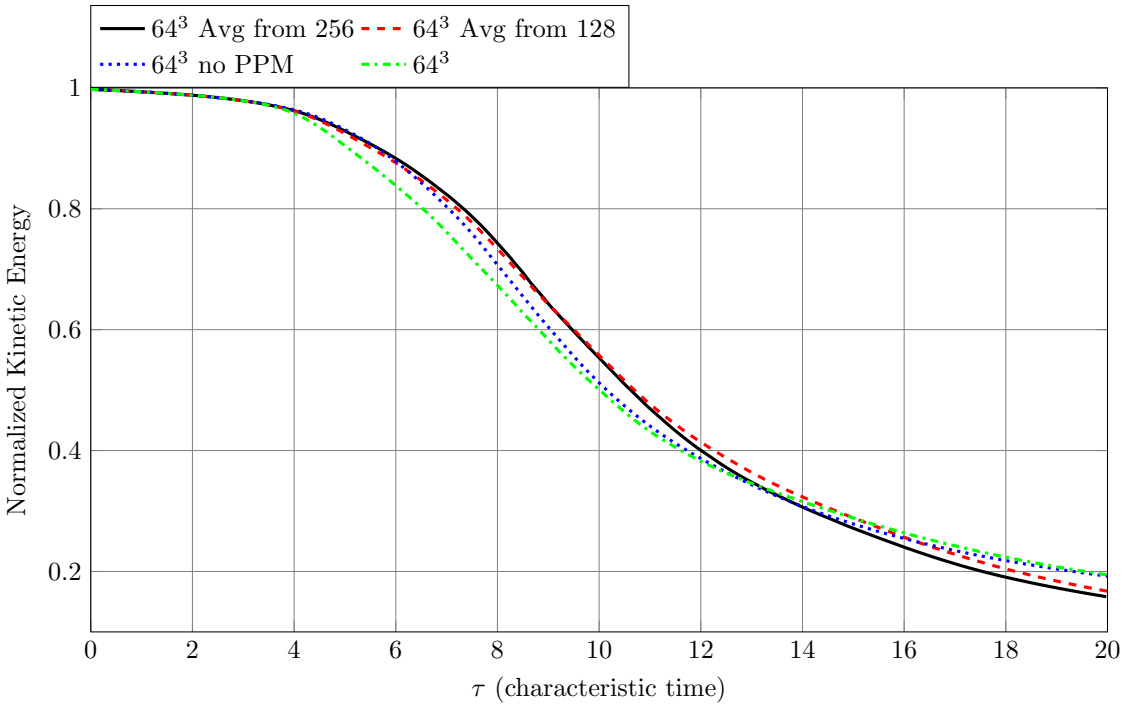

Figure 2: Kinetic energy over time for the Taylor-Green vortex case: baseline comparison

V. Discussion

First, by examining Figs. 2, 3, and 4, it is established that the resolved scales of the 64^3 simulations are grid dependent. It can be observed that the results from the averaged-down 256^3 and 128^3 cases differ significantly from the direct 64^3 results. However, it can also be observed that the averaged down 256^3 and 128^3 results do not differ from one another significantly, suggesting the averaged information is nearly grid converged. It could be expected that an even finer solution (e.g. 512^3) averaged down would produce almost the same result. This would indicate that an accurate representation of the resolved scales at 64^3 could be obtained from using the 128^3 result averaged to 64^3. The goal of the model is to reproduce the results from the averaged-down 256^3 case when solving on a 64^3 mesh.

Considering the effect of the PPM limiter on the quantities of interest, it is apparent that the limiter introduces dissipation into the simulations as would be expected. Curiously, it can be seen in Fig. 3 that the domain-summed enstrophy of the 64^3 case run without the PPM limiter generally follows the trend of the averaged-down cases. It does, however, over-predict from $\tau = 4 - 8$, and under-predict from $\tau = 8$ to the end of the simulation. Additionally, the peak value of the 64^3 case run without the limiter matches the peak value of the averaged-down cases quite well.

While it is important to consider the results that are obtained using a fourth-order central scheme without a limiter mechanism, it is also important to recognize that simulations of many turbulent flows of interest require a limiter for numerical stability. Although the Taylor-Green vortex is a smooth flow at sufficient resolution, 64^3 proved to be just "discontinuous" enough to result in a solution field (not included here) that was somewhat "grainy" in appearance when the limiter was not used.

It is also to be noted that while the results of the 64^3 case show an initial kinetic energy dissipation rate that is too large, they also exhibit a final dissipation rate that is too small. The resulting over-prediction of kinetic energy in the domain at the end of the simulation is intriguing given that, by the end of the simulation, a substantial portion of the energy has been dissipated by viscous effects. Even the limiter did not introduce enough to dissipation to sufficiently reduce the kinetic energy at the end of the simulation. Reasonable explanations include a pile-up of energy at the grid-cutoff scale due to the under-prediction of SGS kinetic energy dissipation coming from SGS turbulence. This would further suggest that running this case at 64^3 resolution without a turbulence model would be insufficient to account for the SGS turbulence when the turbulence has broken down to a sufficiently fine scale (as is seen at the end of the simulation). Furthermore, it

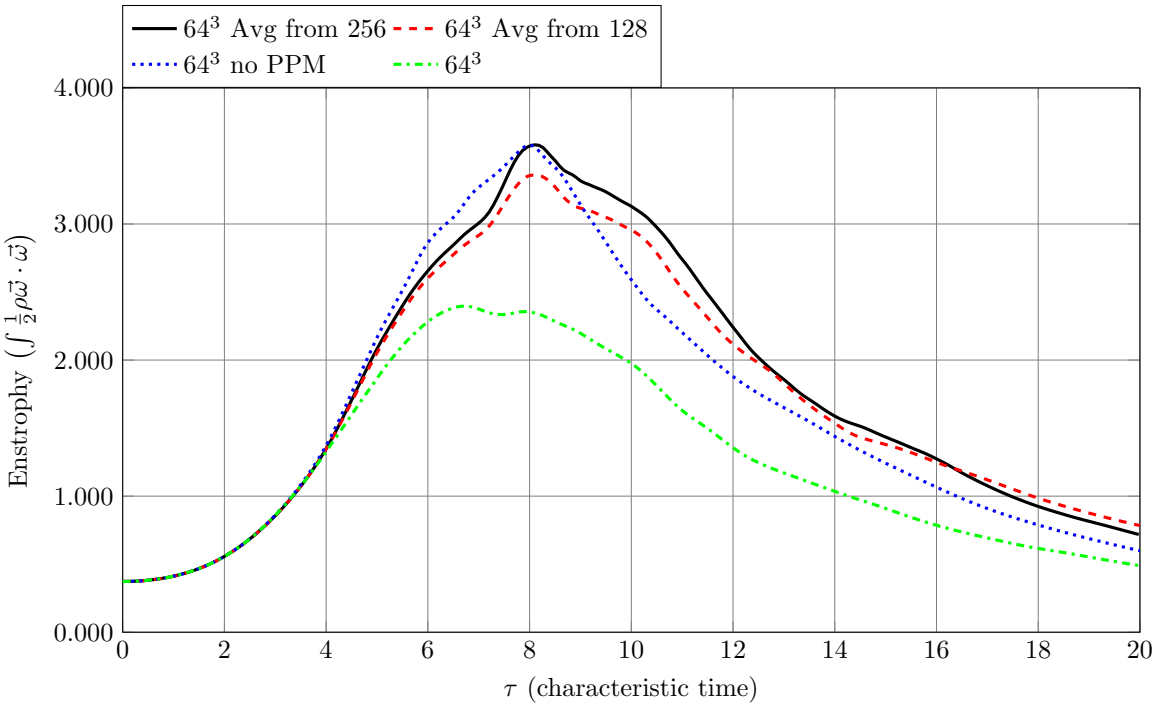

Figure 3: Enstrophy over time for the Taylor-Green vortex case: baseline comparison

would also suggest that an explicit filtering of the solution data is needed during the simulation to remove the influence of the numerical scheme on the resulting solution. Through the use of explicit filtering, the limiter would not excessively dissipate the highest frequency information on the mesh as it would be resolvable by the numerical scheme. The information that is barely resolvable on the mesh would be continually removed.

The second and third sets of figures provide a means by which the various models of subgrid vortex orientation can be compared. From both sets of data, it is readily apparent that the truncated form of Model (1b) with $\sigma = 1$, Eq. 19, is the most dissipative of the orientation models. When a proportion constant $\sigma = 0$ is used, the result is seen to be slightly less dissipative and $\sigma = 0.5$ is seen to be in between the two extremes of $\sigma = 1$ and $\sigma = 0$. Each of these models provides dissipation that is required to model the transfer of kinetic energy from the large scales to the small scales. However, it is reasonable to question whether or not these models are necessary in a case where sufficient dissipation is already being provided by the numerical algorithm such as during the inertial dominated phase of the Taylor-Green problem. For any cases in which the numerical scheme provides insufficient dissipation of near-subgrid-scales, it is expected that improved results are obtained when using one of these SGS models.

The last model, presented in Eq. 35, is, interestingly enough, anti-dissipative. Although it is formulated in a manner somewhat similar to molecular dissipation, it still provides feedback from the small scales that adds to the vorticity. In fact, it can be seen in Fig. 8 that without the limiter, this model initially (form $\tau = 4 - 6$) over-predicts the kinetic energy unlike any of the other models. Although this is not a desirable trait if a limiter is not being utilized, it very well may be of some benefit in circumstances where a limiter is used.

Finally, it is observed from Figs. 7 and 10 that all of the simulations on the 64^3 mesh had too high of a kinetic energy dissipation rate during the early phase of the simulation ($\tau = 4 - 8$), and too high of a dissipation rate during later portions of the simulations ($\tau = 8 - 14$). The early dissipation is likely due to the numerical scheme and could potentially be alleviated through the use of explicit filtering. If the early dissipation was decreased, the turbulence models could potentially provide the correct dissipation at later times in the simulation when it was required (as the smallest turbulent scales increased). All of this will be tested with explicit filtering in the immediate future.

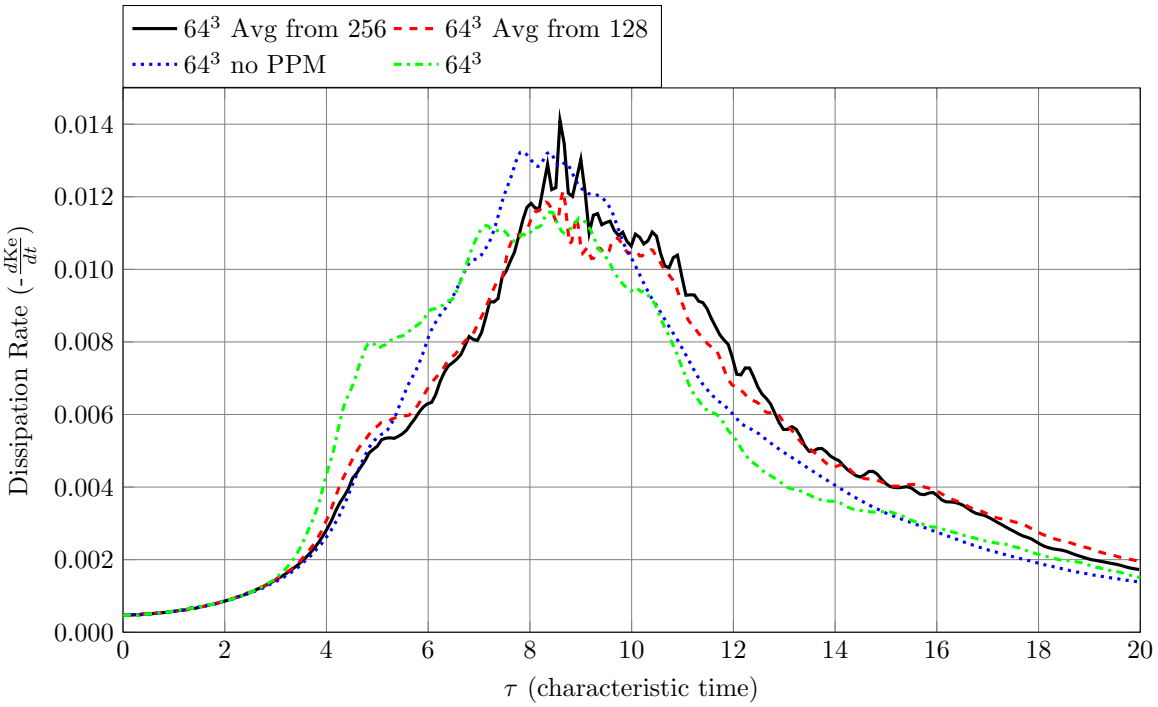

Figure 4: Dissipation rate over time for the Taylor-Green vortex case: baseline comparison

VI. Conclusion

The stretched-vortex subgrid-scale model was found to provide necessary dissipation arising from subgrid-scale turbulence. Additionally, it was shown that the subgrid-vortex orientation vector significantly impacts the simulation results. While orientation with the most extensional eigenvector of the strain-rate tensor was found to provide the most dissipation and alignment with the resolved-scale vorticity vector was found to provide less dissipation, the alignment model derived from the multiplication of the strain-rate tensor with itself was found to be anti-dissipative. The ideal model for a spectral algorithm would not necessarily be best for a non-spectral algorithm, and as a result, it is unknown which of these models would be best when explicit filtering is utilized.

Immediate follow-up research will focus on obtaining additional quantitative results and explicitly filtering the data during the simulations. The explicit filtering will be used to further assess the performance of the stretched-vortex model as a subgrid-scale or sub-analytical-scale model. Additional follow-up research will include the application of these models to forced homogeneous isotropic turbulence cases.

VII. Acknowledgment

This research was supported by the National Science Foundation under the award number 1723066. This material is partly based upon work at LBNL supported by the U.S. Department of Energy, Office of Science, Advanced Scientific Computing Research, under contract number DE-AC02-05CH11231.

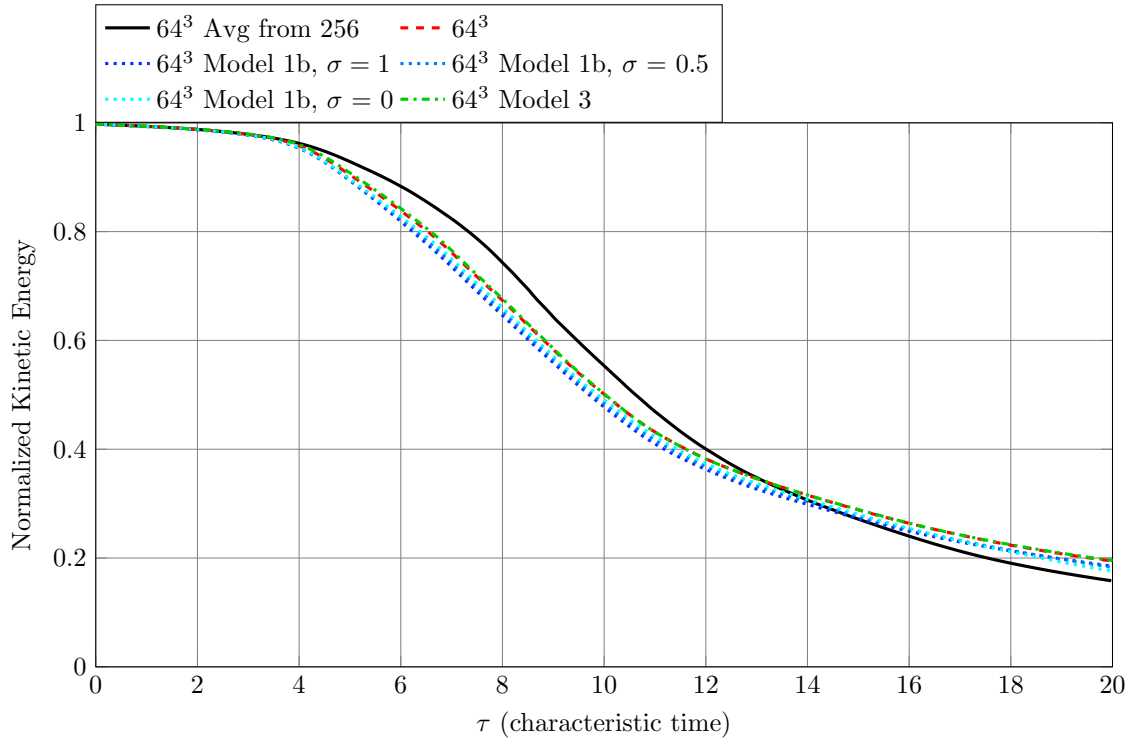

Figure 5: Kinetic energy over time for the Taylor-Green vortex case with PPM: model comparison

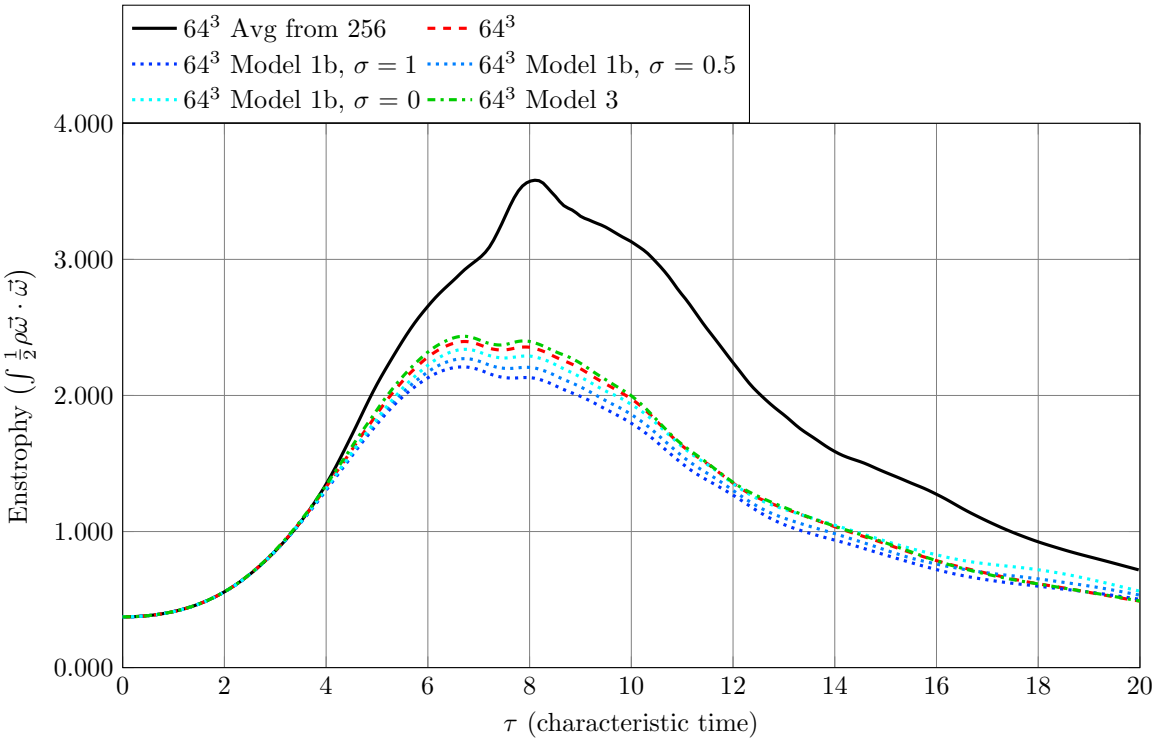

Figure 6: Enstrophy over time for the Taylor-Green vortex case with PPM: model comparison

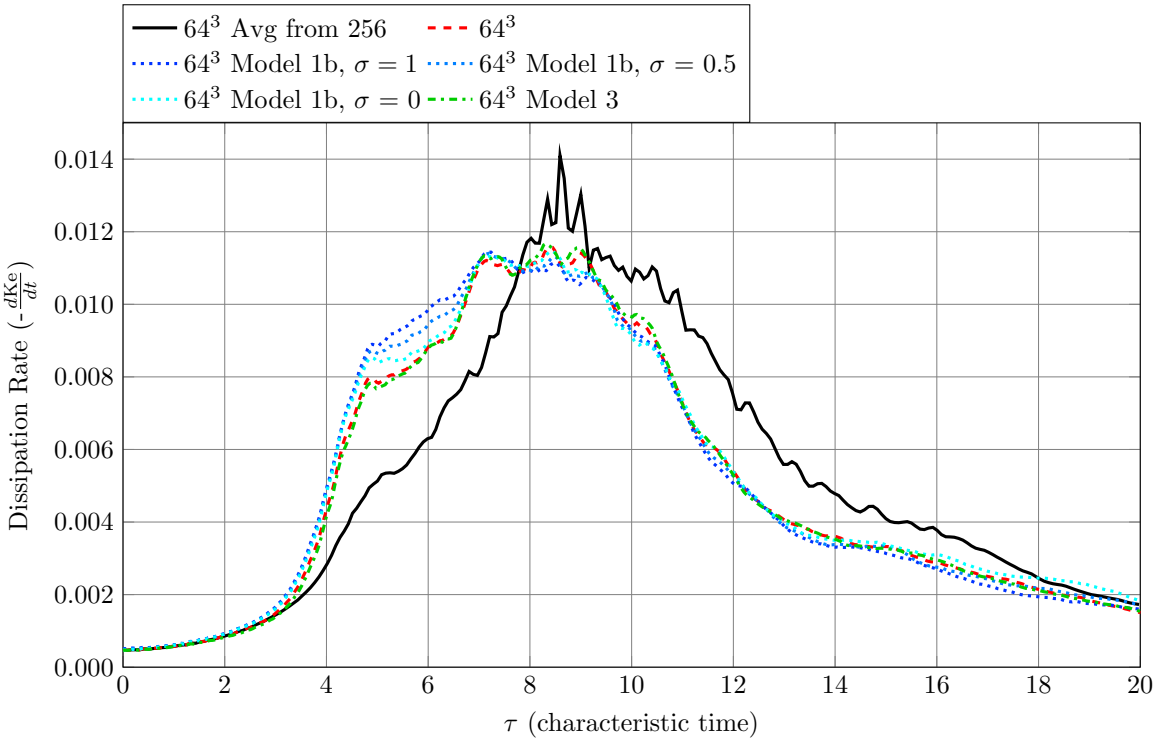

Figure 7: Dissipation rate over time for the Taylor-Green vortex case with PPM: model comparison

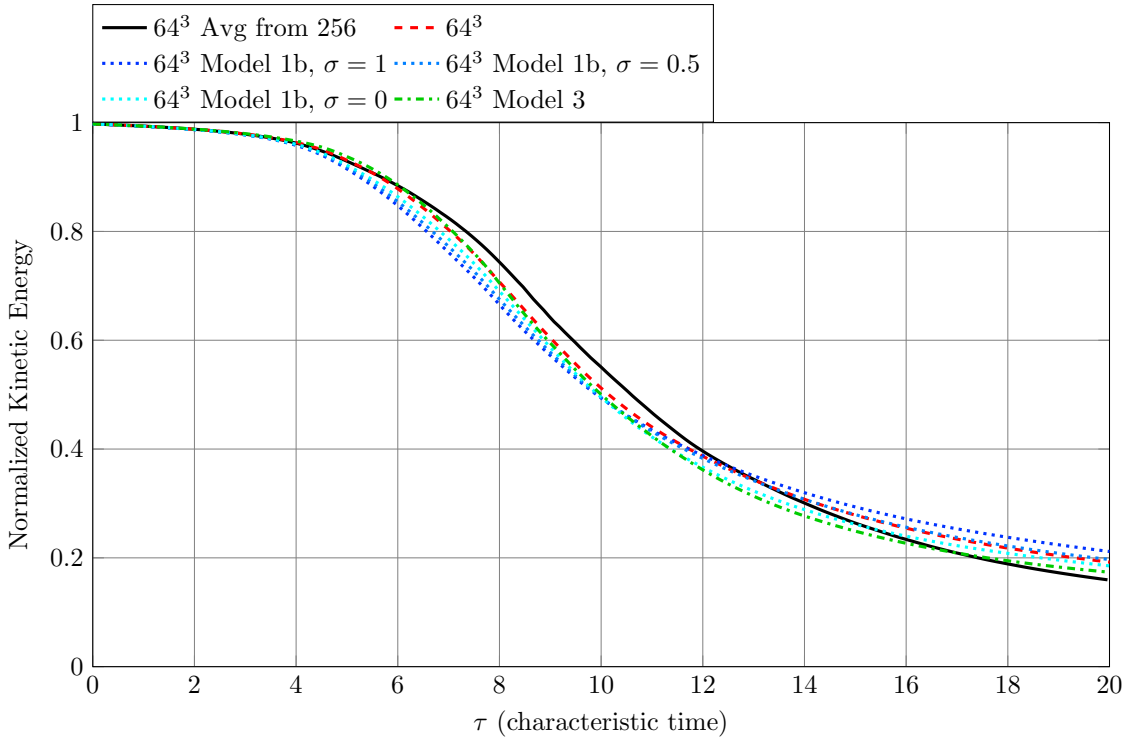

Figure 8: Kinetic energy over time for the Taylor-Green vortex case without PPM: model comparison

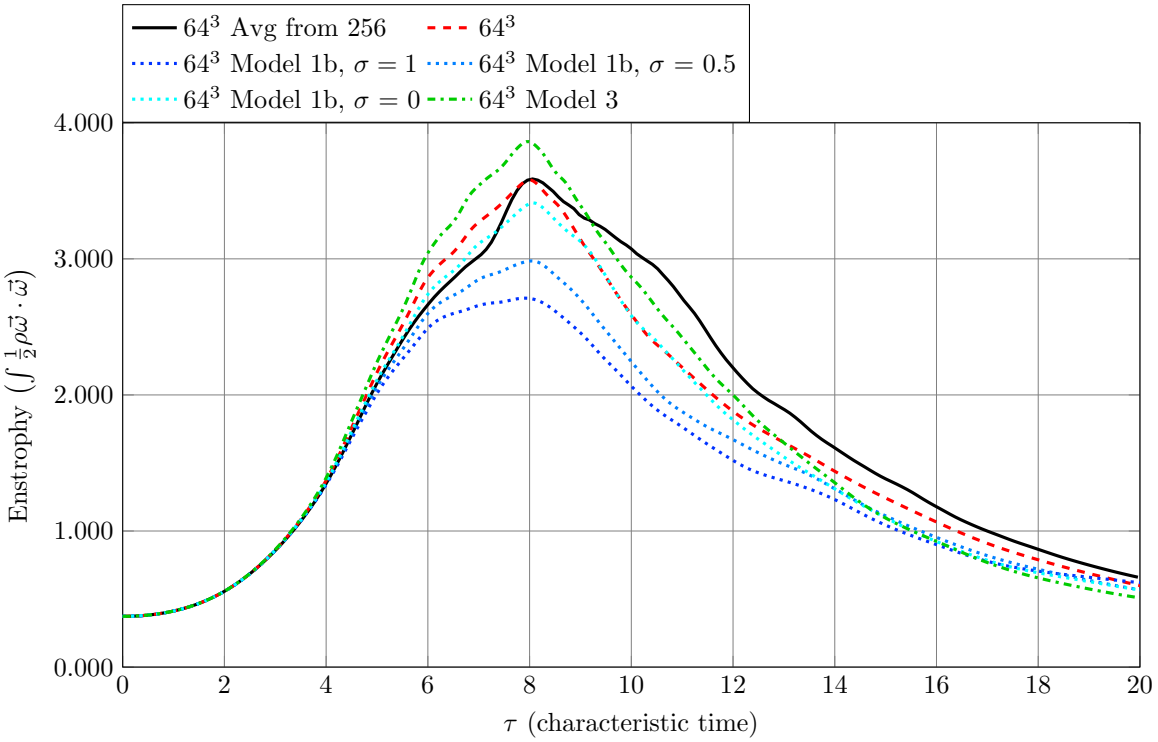

Figure 9: Enstrophy over time for the Taylor-Green vortex case without PPM: model comparison

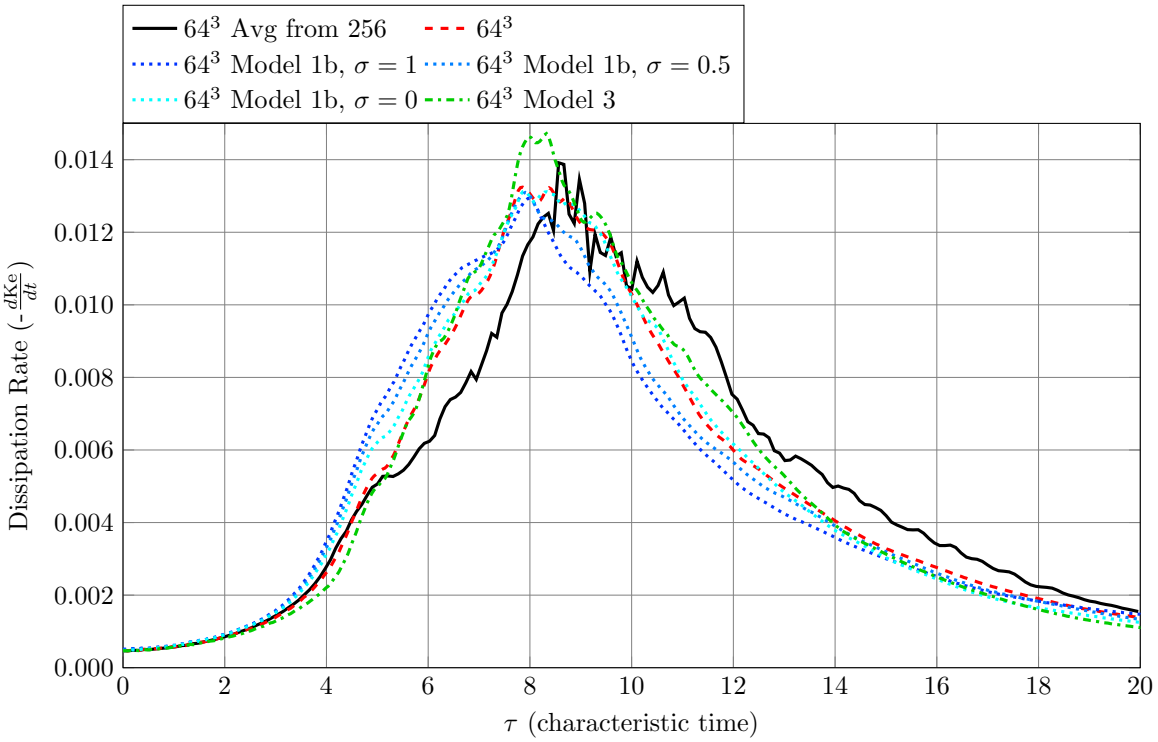

Figure 10: Dissipation rate over time for the Taylor-Green vortex case without PPM: model comparison

References

[1]Sagaut, P., *Large Eddy Simulation for Incompressible Flows*, Springer, 3rd ed., 2005.

[2]Hohlfeld, R. G., King, J. I. F., Drueding, T. W., and Sandri, G. v. H., "Solution of Convolution Integral Equations by the Method of Differential Inversion," *SIAM J. Appl. Math.*, Vol. 53, No. 1, Feb. 1993, pp. 154–167.

[3]Yin, S., Guzik, S., and Gao, X., "A Fourth-Order Finite-Volume Method with Adaptive Mesh Refinement for Large-Eddy Simulation: Wall-Layer Models," *2018 AIAA Aerospace Sciences Meeting*, No. AIAA 2018-1304, AIAA SciTech Forum, 2018, https://doi.org/10.2514/6.2018-1304.

[4]Kolmogorov, A. N., "The local structure of turbulence in incompressible viscous fluid for very large Reynolds numbers," *Dokl. Akad. Nauk SSSR*, Vol. 30, No. 4, 1941, pp. 299–303.

[5]Lundgren, T. S., "Strained spiral vortex model for turbulent fine structure," *Phys. Fluids*, Vol. 25, No. 12, December 1982, pp. 2193–2203.

[6]Pullin, D. I. and Saffman, P. G., "Vortex Dynamics in Turbulence," *Annual Review of Fluid Mechanics*, Vol. 30, 1998, pp. 31–51.

[7]Pullin, D. I. and Saffman, P. G., "On the Lundgren-Townsend model of turbulent fine scales," *Physics of Fluids*, Vol. 5, No. 1, January 1993, pp. 126–145.

[8]Pullin, D. I. and Saffman, P. G., "Reynolds stresses and one-dimensional spectra for a vortex model of homogeneous anisotropic turbulence," *Physics of Fluids*, Vol. 6, No. 5, May 1994, pp. 1787–1796.

[9]Pullin, D. I., Buntine, J. D., and Saffman, P. G., "On the spectrum of a stretched spiral vortex," *Physics of Fluids*, Vol. 6, No. 9, September 1994, pp. 3010–3027.

[10]Saffman, P. G. and Pullin, D. I., "Anisotropy of the Lundgren-Townsend model of fine-scale turbulence," *Physics of Fluids*, Vol. 6, No. 2, February 1994, pp. 802–807.

[11]Misra, A. and Pullin, D. I., "A vortex-based subgrid stress model for large-eddy simulation," *Physics of Fluids*, Vol. 9, No. 8, August 1997, pp. 2443–2454.

[12]Chung, D. and Pullin, D. I., "Direct numerical simulation and large-eddy simulation of stationary buoyancy-driven turbulence," *J. Fluid Mechanics*, Vol. 643, 2010, pp. 279–308.

[13]Mattner, T. W., "A refined stretched-vortex model for large-eddy simulation of turbulent mixing layers," Afmc, 17th Australasian Fluid Mechanics Conference, December 2010.

[14]Mattner, T. W., "Large-eddy simulations of turbulent mixing layers using the stretched vortex model," *J. Fluid Mechanics*, Vol. 671, 2011, pp. 507–534.

[15]Voelkl, T., Pullin, D. I., and Chan, D. C., "A physical-space version of the stretched-vortex subgrid-stress model for large-eddy simulation," *Physics of Fluids*, Vol. 12, No. 7, July 2000, pp. 1810–1825.

[16]Pullin, D. I. and Lundgren, T. S., "Axial motion and scalar transport in stretched spiral vortices," *Physics of Fluids*, Vol. 13, No. 9, September 2001, pp. 2553–2563.

[17]Pullin, D. I., "A vortex-based model for the subgrid flux of a passive scalar," *Physics of Fluids*, Vol. 12, No. 9, September 2000, pp. 2311–2319.

[18]Kosovic, B., Pullin, D. I., and Samtaney, R., "Subgrid-scale modeling for large-eddy simulations of compressible turbulence," *Physics of Fluids*, Vol. 14, No. 4, April 2002, pp. 1511–1522.

[19]Hill, D. J., Pantano, C., and Pullin, D. I., "Large-eddy simulation and multi-scale modelling of a Richtmyer-Meshkov instability with reshock," *J. Fluid Mechanics*, Vol. 557, 2006, pp. 29–61.

[20]Chung, D. and Pullin, D. I., "Large-eddy simulation and wall modelling of turbulent channel flow," *J. Fluid Mechanics*, Vol. 631, 2009, pp. 281–309.

[21]Cheng, W. and Samtaney, R., "Physics of Fluids," *Power-law versus log-law in wall-bounded turbulence: A large-eddy simulation perspective*, Vol. 26, 2014, pp. 011703–1–011703–7.

[22]Cheng, W., Pullin, D. I., and Samtaney, R., "Large-eddy simulation of separation and reattachment of a flat plate turbulent boundary layer," *J. Fluid Mechanics*, Vol. 785, 2015, pp. 78–108.

[23]Cheng, W., Pullin, D. I., and Samtaney, R., "Large-eddy simulation of flow over a grooved cylinder up to transcritical Reynolds numbers," *J. Fluid Mechanics*, Vol. 835, 2018, pp. 327–362.

[24]Gao, X., Guzik, S. M. J., and Colella, P., "Fourth Order Boundary Treatment for Viscous Fluxes on Cartesian Grid Finite-Volume Methods," AIAA 2014-1277, 52nd AIAA Aerospace Sciences Meeting, 2014.

[25]Guzik, S. M., Gao, X., Owen, L. D., McCorquodale, P., and Colella, P., "A Freestream-Preserving Fourth-Order Finite-Volume Method in Mapped Coordinates with Adaptive-Mesh Refinement," *Comput. Fluids*, Vol. 123, 2015, pp. 202–217.

[26]Guzik, S. M., Gao, X., and Olschanowsky, C., "A high-performance finite-volume algorithm for solving partial differential equations governing compressible viscous flows on structured grids," *Comput. Math Appl.*, Vol. 72, 2016, pp. 2098–2118.

[27]Gao, X., Owen, L. D., and Guzik, S. M. J., "A Parallel Adaptive Numerical Method with Generalized Curvilinear Coordinate Transformation for Compressible Navier-Stokes Equations," *Int. J. Numer. Meth. Fluids*, Vol. 82, 2016, pp. 664–688.

[28]Owen, L. D., Guzik, S. M., and Gao, X., "A high-order adaptive algorithm for multispecies gaseous flows on mapped domains," *Comput. Fluids*, Vol. 170, 2018, pp. 249 – 260.

[29]Shetty, D. A. and Frankel, S. H., "Assessment of stretched vortex subgrid-scale models for LES of incompressible inhomogeneous turbulent flows," *Int. J. Numer. Meth. Fluids*, Vol. 73, 2013, pp. 152–171.

[30]Clark, R. A., Ferziger, J. H., and Reynolds, W. C., "Evaluation of subgrid-scale models using an accurately simulated turbulent flow," *J . Fluid Mechanics*, Vol. 91, 1979, pp. 1–16.

[31]Margolin, L. G., "Finite-scale equations for compressible fluid flow," *Phil. Trans. R. Soc. A*, Vol. 367, 2009, pp. 2861–2871.

[32]Bull, J. R. and Jameson, A., "Simulation of the Compressible Taylor Green Vortex using High-Order Flux Reconstruction Schemes," *7th AIAA Theoretical Fluid Mechanics Conference*, No. AIAA 2014-3210, AIAA AVIATION Forum, 2014.